

An Orally Administered CeO₂@Montmorillonite Nanozyme Targets Inflammation for Inflammatory Bowel Disease Therapy

Sheng Zhao, Yixuan Li, Quanyi Liu, Sirong Li, Yuan Cheng, Chaoqun Cheng, Ziyang Sun, Yan Du, Christopher J. Butch,* and Hui Wei*

Safe, effective, and convenient administration of therapeutic nanomaterials is one of the greatest difficulties in nanomedicine. To tackle this challenge, a system which couples multi-enzyme mimicking CeO₂ nanoparticles with clinically approved montmorillonite (MMT) for inflammatory bowel disease (IBD) therapy is reported. CeO₂ exhibits superoxide dismutase- and catalase-like activities, and hydroxyl radical scavenging activity, making it more efficient at scavenging reactive oxygen species (ROS) than non-catalytic antioxidants while being more stable than free enzymes. In addition, negatively-charged MMT can be orally administered and specifically adsorbed onto positively-charged inflamed colon tissue via electrostatic interactions for targeted delivery. When the two are assembled together by in situ growth of CeO₂ onto MMT, the optimized CeO₂@MMT(1:9) is stable in the stomach for oral delivery, targets the inflamed colon through electrostatic interactions, and reduces inflammation through ROS scavenging, all without any significant systemic exposure as demonstrated by the relief of murine IBD in vivo.

the condition can lead to more serious (and more lethal) diseases such as colon cancer.^[2] Current clinical therapies based on small molecular drugs, antibiotics, and antibodies are not completely effective^[3] and long-term use may even cause severe complications, antibiotic resistance, and immunological response.^[4] The difficulties in treating IBD can be partially attributed to the lack of specificity of the treatments; risk of side effects is increased both with increased dosage, and wider systemic exposure to the treatment. Consequently, numerous targeted IBD therapies have been attempted, including pH-, pressure-, and time-dependent delivery systems.^[5] While some of these systems target the whole colon, most are dependent on delivery via the bloodstream, and few are truly specific to the disease location, the

1. Introduction


Inflammatory bowel disease (IBD) is a refractory chronic disease which in 2017 caused 38 000 deaths among 6.8 million patients.^[1] Prevalence of IBD is highest in developed countries, with rates upward of 250 per 100 000 in some age groups, and a worldwide, all ages, prevalence of 84.3 per 100 000, 5% higher than in 1990.^[1] Though deaths directly attributable to IBD are low, IBD patients' quality of life is significantly decreased and

inflamed colonic lesions. Therefore, innovative targeting strategies which can localize treatment to the site of the inflammation are still greatly needed.

The inflamed colon is characterized by an enrichment of positively charged proteins and elevated levels of reactive oxygen species (ROS).^[6] A therapeutic strategy which can target these positively charged proteins through negatively charged drugs and drug carriers and scavenge ROS to alleviate inflammation could then be an extremely effective treatment for

S. Zhao, S. Li, Dr. Y. Cheng, C. Cheng, Prof. C. J. Butch, Prof. H. Wei
 College of Engineering and Applied Sciences
 Nanjing National Laboratory of Microstructures
 Jiangsu Key Laboratory of Artificial Functional Materials
 Nanjing University
 Nanjing, Jiangsu 210093, China
 E-mail: chrisbutch@nju.edu.cn; weihui@nju.edu.cn

Dr. Y. Li, Z. Sun
 State Key Laboratory of Pharmaceutical Biotechnology
 Department of Sports Medicine and Adult Reconstructive Surgery
 Nanjing Drum Tower Hospital
 The Affiliated Hospital of Nanjing University Medical School
 Nanjing, Jiangsu 210008, China

 The ORCID identification number(s) for the author(s) of this article can be found under <https://doi.org/10.1002/adfm.202004692>.

DOI: 10.1002/adfm.202004692

Q. Liu, Prof. Y. Du
 State Key Laboratory of Electroanalytical Chemistry
 Changchun Institute of Applied Chemistry
 Chinese Academy of Sciences
 Changchun, Jilin 130022, China

Q. Liu, Prof. Y. Du
 University of Science and Technology of China
 Hefei, Anhui 230026, China

Prof. H. Wei
 State Key Laboratory of Analytical Chemistry for Life Science
 and State Key Laboratory of Coordination Chemistry
 School of Chemistry and Chemical Engineering
 Nanjing University
 Nanjing, Jiangsu 210023, China

Prof. H. Wei
 Chemistry and Biomedicine Innovation Center (ChemBIC)
 Nanjing University
 Nanjing, Jiangsu 210023, China

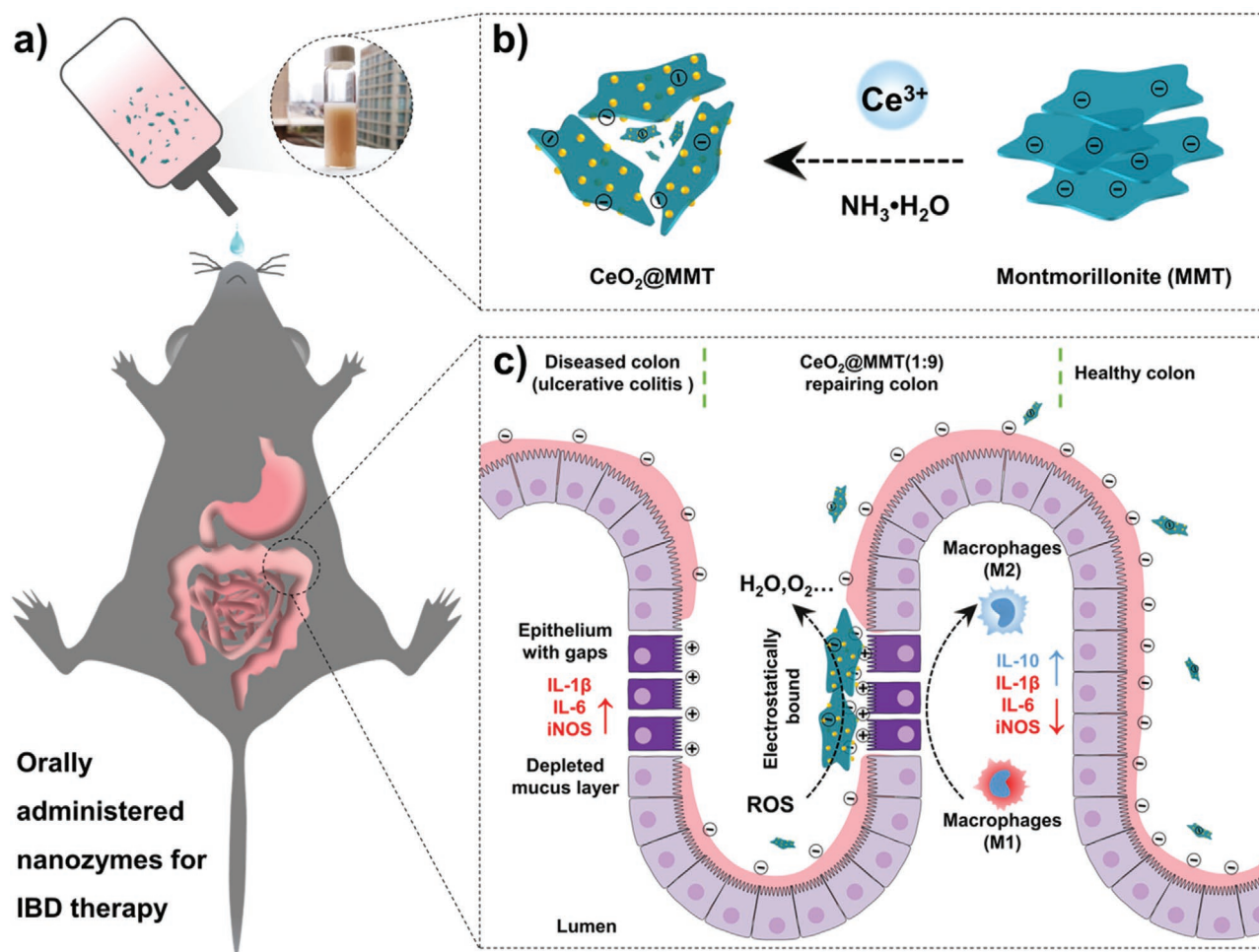


Figure 1. Design and synthesis of orally administered $\text{CeO}_2\text{@MMT}$ to target inflamed colon for treating inflammatory bowel disease (IBD). a) $\text{CeO}_2\text{@MMT}$ is orally administered to treat mice with IBD. b) Synthetic scheme of $\text{CeO}_2\text{@MMT}$ by in situ growth of ceria nanoparticles (CeO_2 NPs) onto MMT sheets. c) Therapeutic effects of $\text{CeO}_2\text{@MMT}$ on IBD. Left: Abnormalities of ulcerative colitis include mucus depletion, accumulation of positively charged proteins, increased permeability of the epithelial cell layer, increased levels of ROS and pro-inflammatory macrophages (M1), as well as upregulation of cytokines (IL-1 β , IL-6, iNOS, etc.). Middle: The negatively charged $\text{CeO}_2\text{@MMT}$ (1:9) specifically targets the positively charged inflamed colon. When electrostatically bound, $\text{CeO}_2\text{@MMT}$ scavenges elevated ROS via the multiple enzyme-like activities of CeO_2 NPs. Right: After the intervention of $\text{CeO}_2\text{@MMT}$ (1:9), the damaged intestinal epithelial barrier is partially repaired, while pro-inflammatory macrophages (M1) and cytokines (IL-1 β , IL-6, iNOS, etc.) are reduced, anti-inflammatory macrophages (M2) and cytokines (e.g., IL-10) are increased.

this disease.^[7] In one example, to harness these pathophysiological features, ROS scavenging enzymes (i.e., superoxide dismutase (SOD) and catalase) encapsulated within negatively charged liposomes were fabricated to treat IBD via intracolonic administration.^[7a,8] Unfortunately, natural enzymes are neither stable nor eco-efficient, and many of them cause immunological response while having catalytic activity against just one of many ROS.^[9] Recently a more facile treatment was developed by loading an anti-inflammatory drug, dexamethasone, into a negatively charged hydrogel for inflammation-targeting therapy.^[6a] However, this treatment must be delivered by enema which may compromise patients' compliance and cannot reach inflammation of the upper colon or be administered to patients with diarrhea.^[6a]

To tackle these challenges, we have designed a nanozyme with a formulation of $\text{CeO}_2\text{@MMT}$ suitable for oral administration, and which directly targets the inflamed colon through

electrostatic interactions for specific IBD treatment. Synthesis of $\text{CeO}_2\text{@MMT}$ was conducted by in situ growth of ceria nanoparticles (CeO_2 NPs) on sheets of montmorillonite (MMT) (Figure 1b). Nanoceria is a multi-enzyme mimic with both SOD- and CAT-like activities as well as hydroxyl radical scavenging activity. This catalytic anti-oxidant activity makes nanoceria a potent treatment for various diseases including inflammatory diseases through ROS elimination.^[10] Despite great promise, it remains challenging to develop orally administered CeO_2 NPs for treating IBD. This is mainly because the positive charges of CeO_2 NPs impart no specificity toward the inflamed colon while the ultra-small sizes allow their rapid absorption through the gastrointestinal wall increasing systemic exposure and leading to undesired side effects.^[11] In contrast, MMT is a natural negatively-charged layered material,^[12] which is well tolerated by the digestive tract and has been clinically used to alleviate diarrhea through physical binding, covering of mucosa,

and removal of toxins.^[13] Unlike CeO₂ NPs, MMT cannot pass through the gastrointestinal barrier and is excreted from the body along with any absorbed toxins. Notably, MMT does not interfere with normal colonic function either.^[13a] In this regard, MMT is an ideal substrate to compensate the potential drawbacks of CeO₂ NPs, while CeO₂ NPs can impart MMT with anti-ROS capabilities.

Here we demonstrate that CeO₂ NPs grown in situ on MMT sheets confer ROS scavenging (i.e., anti-inflammatory) activity to the MMT sheets, while the MMT sheets significantly minimize the systemic absorption of CeO₂ NPs and thus reduce their potential nanotoxicity. We show that when administered orally, CeO₂@MMT is stable in the stomach and targets the inflamed colon via electrostatic interactions with negligible systemic absorption. Finally, we demonstrate that the CeO₂@MMT adsorbed at the colonic lesions scavenges excess ROS, thus reducing inflammation at the diseased sites, while promoting anti-inflammatory immune response, and, ultimately, effectively treating dextran sulfate sodium (DSS)-induced IBD in murine models (Figure 1a,c).

2. Results

2.1. Synthesis and Characterization of CeO₂@MMT

The CeO₂@MMT nanozymes were synthesized by in situ growth of CeO₂ NPs onto MMT sheets (Figure 1b). First, due to the sensitivity of the layered Si–O structure of MMT sheets to alkaline and cationic synthetic conditions,^[12b,14] the effects of ammonia and Ce³⁺ on the structural integrity of MMT were studied. As the X-ray diffraction (XRD) patterns and transmission electron microscopy (TEM) images shown in Figures S1 and S2, Supporting Information, ammonia and Ce³⁺ showed negligible effect on the MMT structure.

Next, CeO₂ NPs were grown in situ on MMT sheets (CeO₂@MMT) by adding a glycol solution of 12.6 mg mL⁻¹ Ce(NO₃)₃·6H₂O to a suspension of MMT, at either 20 or 50 mg mL⁻¹ in a 1:1 ratio. Based on the ratio (w:w) of ceria to MMT in CeO₂@MMT (Figure S3, Supporting Information), we refer to the product nanozymes as CeO₂@MMT(2:8) and CeO₂@MMT(1:9), respectively. The formation of CeO₂@MMT nanozymes was first confirmed by using TEM imaging. As shown in Figure 2a, uniform and discrete ultra-small CeO₂ NPs were observed on the MMT sheets. Compared with free CeO₂ NPs, CeO₂ NPs loaded on MMT sheets had better dispersion and smaller sizes (3.5 ± 0.7, 2.5 ± 0.5, and 1.6 ± 0.2 nm for CeO₂, CeO₂@MMT(2:8), and CeO₂@MMT(1:9), respectively) (Figure 2a,b), which could be explained by the effect of heterogeneous nucleation.^[15] Si, Al, O, and Ce element mapping of CeO₂@MMT nanozymes by scanning electron microscopy (SEM) with energy-dispersive spectroscopy (EDS) further confirmed that CeO₂ NPs were evenly dispersed onto the MMT sheets (Figures S4 and S5, Supporting Information). The crystalline features of the nanozymes were characterized by using XRD. As shown in Figure 2c, the characteristic peaks of ceria at 2θ = 28.5°, 32.9°, 47.4°, and 56.8° were observed for CeO₂@MMT(2:8) and CeO₂@MMT(1:9), suggesting that CeO₂ NPs were successfully grown on the MMT sheets.^[16]

Meanwhile, the characteristic peaks of MMT were also observed for CeO₂@MMT(2:8) and CeO₂@MMT(1:9), which confirmed the integrity of MMT after growth of CeO₂ NPs.

Since the enzyme-like activities of ceria are dependent on the ratio of Ce³⁺ to Ce⁴⁺ on their surfaces,^[17] X-ray photoelectron spectra (XPS) were collected to quantify the ratio of the Ce species. As shown in Figure 2b and Figure S6, Supporting Information, both CeO₂@MMT(2:8) and CeO₂@MMT(1:9) had higher Ce³⁺ fractions (42.8% and 50.2%) than free CeO₂ (38.3%). Moreover, the Ce³⁺ fraction of CeO₂@MMT increased with increased MMT content. Interestingly, for CeO₂, CeO₂@MMT(2:8), and CeO₂@MMT(1:9), the Ce³⁺ fraction was inversely correlated with particle size (Figure 2b). This phenomenon may be explained by smaller CeO₂ NPs having larger surface areas ($S_{\text{CeO}_2@\text{MMT}(1:9)}/S_{\text{CeO}_2@\text{MMT}(2:8)}/S_{\text{CeO}_2} = 4.7:2.5:1$) with more oxygen deficiencies, which would significantly enhance the ROS scavenging activity.^[17]

For effective electrostatic targeting of the inflamed colon, the negative charge of MMT must be retained after CeO₂ NPs loading. Therefore, we measured the zeta potentials of MMT before and after loading with CeO₂ NPs. As shown in Figure 2d, the zeta potentials of MMT, CeO₂@MMT(2:8), and CeO₂@MMT(1:9) were all negative charge (i.e., -30.3 ± 1.7, -25.5 ± 0.5, and -29.7 ± 0.5 mV, respectively). With the ratio of CeO₂ NPs to MMT increase, the negative charge of CeO₂@MMT(x:10-x) decreased (Figure S7, Supporting Information). In contrast, the CeO₂ had a positive charge of 35.3 ± 1.0 mV.^[18] We also made CeO₂@halloysite and CeO₂@carbon (edible carbon) by using the same in situ growth method. Although both CeO₂@halloysite and CeO₂@carbon also showed good structural stabilities (Figures S8 and S9, Supporting Information), the weak negative or positive charge hindered their further therapeutic applications (Figure S10, Supporting Information). These results demonstrate that the MMT sheets are capable of screening the positively charged CeO₂ NPs, leading to CeO₂@MMT nanozymes with an overall negative charge capable of targeting positively charged colonic lesions.

2.2. ROS Scavenging Activity of CeO₂@MMT

The ROS scavenging activity of CeO₂@MMT nanozymes toward •O₂⁻, H₂O₂, and •OH, representative ROS involved in IBD, was then investigated (Figure 2e–g). First, the SOD-like activity for •O₂⁻ elimination was studied using a •O₂⁻ specific WST-1 assay kit.^[17] The SOD-like activity of a nanozyme is directly correlated with the amount of •O₂⁻ it can eliminate. As shown in Figure 2e, both CeO₂@MMT(2:8) and CeO₂@MMT(1:9) exhibited slightly better •O₂⁻ eliminating efficiencies when compared with the same weight of CeO₂, indicating their higher SOD-like activities. On the other hand, MMT(8) and MMT(9) showed negligible SOD-like activity, demonstrating that the SOD-like activity of CeO₂@MMT originated from the loaded CeO₂ NPs.

H₂O₂ is produced from •O₂⁻ dismutation and can be further decomposed into H₂O and O₂ by CAT. The CAT-like activity of nanozymes was studied by monitoring the generated O₂ from the catalytic decomposition of H₂O₂ with an oxygen electrode.^[19] As shown in Figure 2f, CeO₂@MMT(2:8) and CeO₂@MMT(1:9) generated nearly the same amounts of O₂ compared with CeO₂, indicating their comparable CAT-like activities.

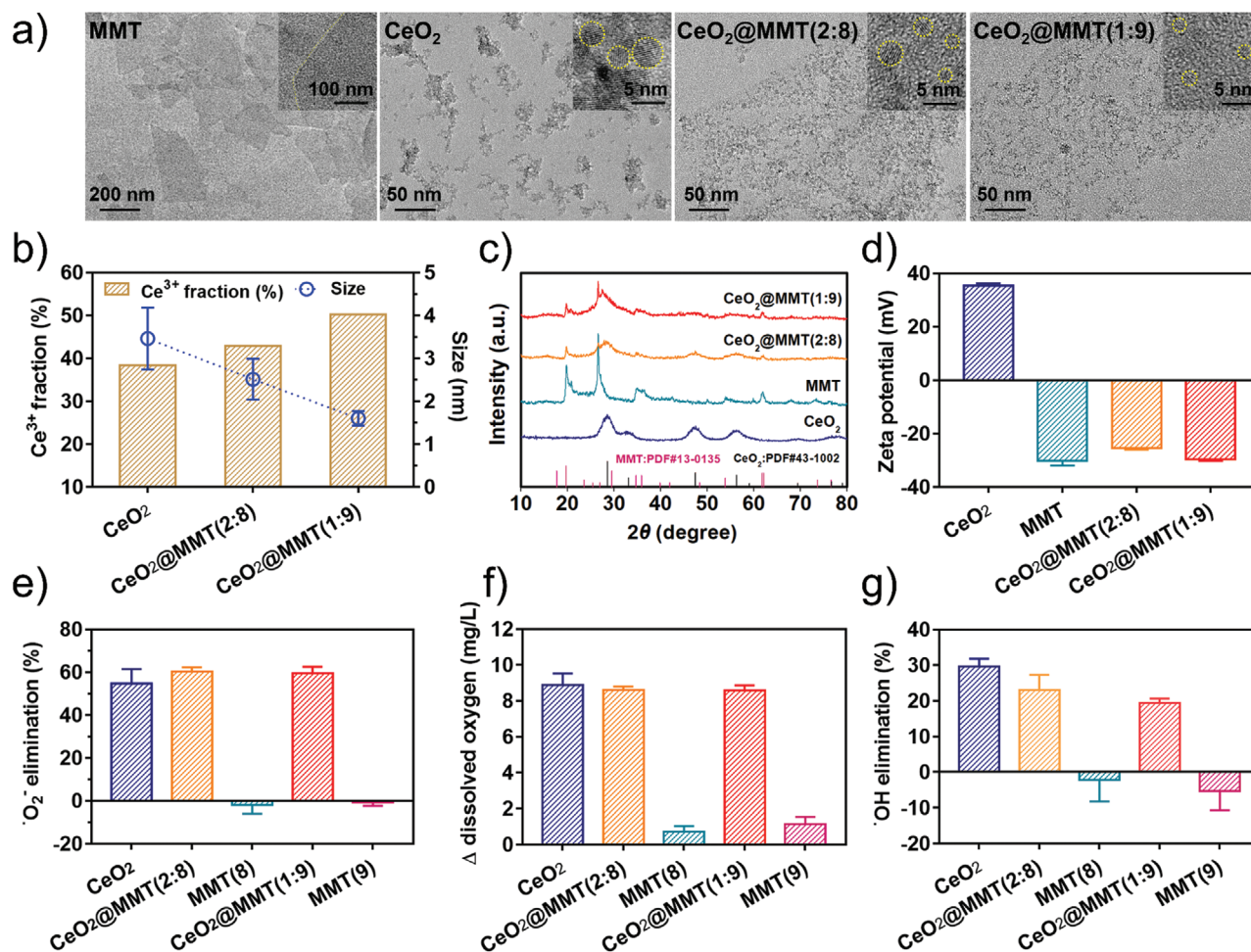


Figure 2. Structure characterization and ROS-scavenging activities of CeO_2 and $\text{CeO}_2@MMT$. a) TEM images. b) Ce^{3+} fraction and particle size. c) XRD patterns. d) Zeta potentials. e) Percentage of superoxide radical elimination catalyzed by SOD-like activity of indicated materials. f) Net oxygen generation from H_2O_2 catalyzed by CAT-like activity of indicated materials. Δ dissolved oxygen = total dissolved oxygen – dissolved oxygen of H_2O_2 self-decomposition. g) Percentage of hydroxyl radical elimination catalyzed by $\cdot\text{OH}$ scavenging activity of indicated materials. e–g) Amounts of materials used were normalized by ceria content. $20 \mu\text{g mL}^{-1}$ of ceria was used for (e) and (g), and $100 \mu\text{g mL}^{-1}$ of ceria was used for (f). MMT(8) and MMT(9) with an equal amount of MMT to $\text{CeO}_2@MMT(2:8)$ and $\text{CeO}_2@MMT(1:9)$, respectively, were used as the control samples to examine the effect of MMT. Data are presented as mean \pm standard error of the mean ($n = 3$).

$\cdot\text{OH}$ is another highly oxidizing ROS that can cause damage to various biomolecules in vivo, though there is no specific enzyme for eliminating $\cdot\text{OH}$.^[20] A nanozyme with $\cdot\text{OH}$ scavenging activity would then provide unique advantages in eliminating ROS build-up. The $\cdot\text{OH}$ scavenging activity of the $\text{CeO}_2@MMT$ species was evaluated by using electron paramagnetic resonance (EPR) spectroscopy with an $\cdot\text{OH}$ specific trapping agent 5,5-dimethyl-1-pyrroline N-oxide (DMPO).^[16] The $\cdot\text{OH}$ scavenging activity is indicated by the amount of $\cdot\text{OH}$ eliminated, which is evaluated via the decrease in EPR signal of the DMPO/ $\cdot\text{OH}$ adduct. As shown in Figure 2g and Figure S11, Supporting Information, both $\text{CeO}_2@MMT(2:8)$ and $\text{CeO}_2@MMT(1:9)$ showed obvious $\cdot\text{OH}$ scavenging activities (OHS), though they were slightly lower than that of CeO_2 . As expected, MMT(8) and MMT(9) did not show $\cdot\text{OH}$ scavenging activities and, in fact, slightly promoted the generation of $\cdot\text{OH}$, which may be due to the trace metal ions in MMT, such as iron (II).^[21]

Overall, both $\text{CeO}_2@MMT(2:8)$ and $\text{CeO}_2@MMT(1:9)$ exhibited high scavenging activities against the three representative ROS. Because the treatment of bowel diseases needs a large dose (3 to 9 g per person per day, which is based on the Provisions of the OTC Chemical Drug Product Template of China), we selected $\text{CeO}_2@MMT(1:9)$ with a higher dose of MMT for the following study.

2.3. $\text{CeO}_2@MMT(1:9)$ Protected Cells from ROS-Induced Damage

After investigating the in vitro ROS scavenging activity of $\text{CeO}_2@MMT(1:9)$, we studied its anti-inflammatory effect on the cellular level. We selected RAW264.7 macrophage cells which are often present in inflamed tissues and HT-29 cells which are a good model of the epithelial tissue of the colon.^[6a,7b] As shown in Figure 3a, two cell culture modes, 1) coin-cubation and 2)

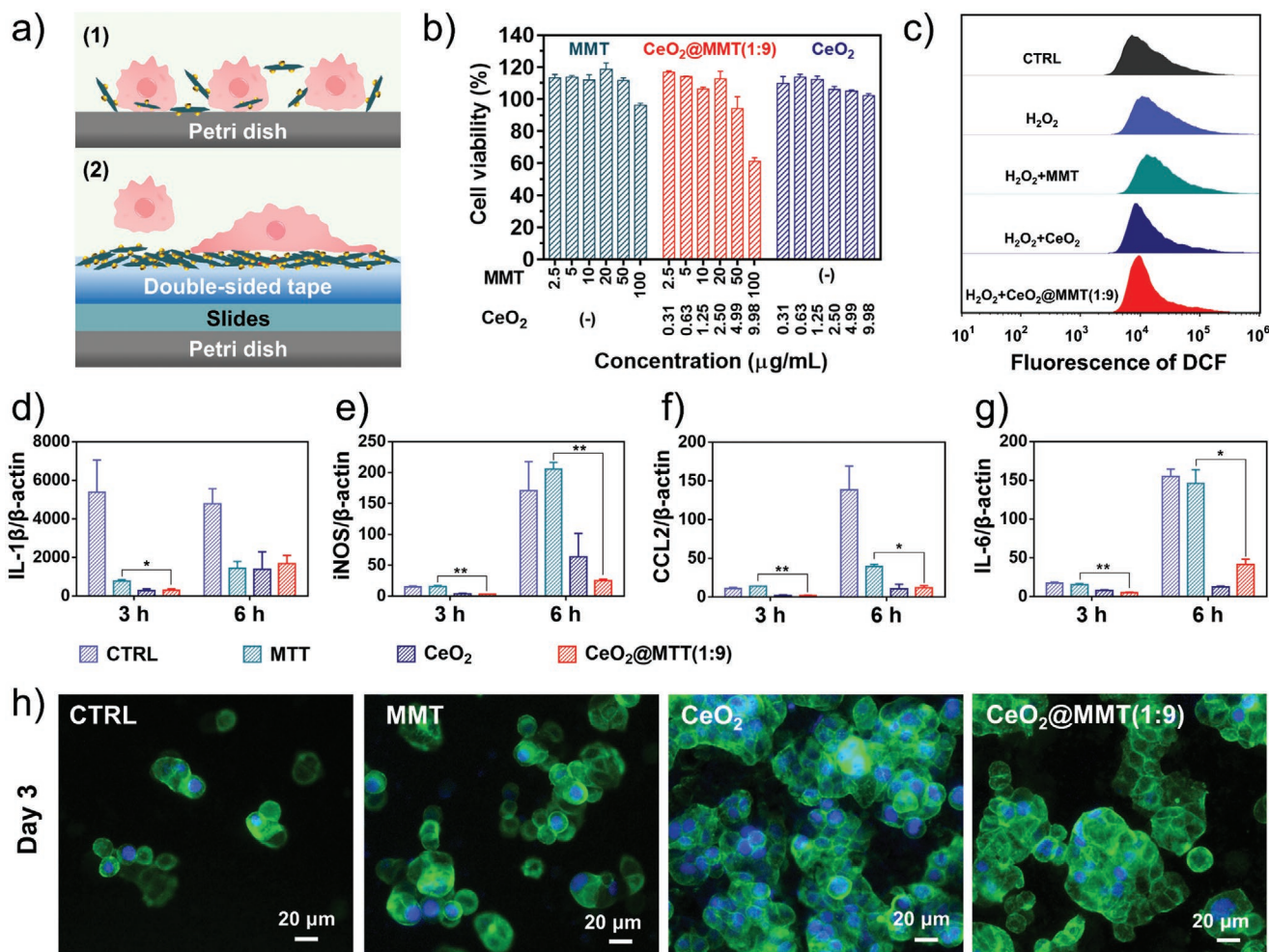


Figure 3. Cell viability, scavenging ROS, and regulating the polarization of macrophages with $\text{CeO}_2@MMT(1:9)$ in vitro. a) Schematic diagram of the interactions of $\text{CeO}_2@MMT(1:9)$ and cells in the 1) coincubation and 2) topical application assays. b) HT-29 cell viability after incubation for 1 day with indicated materials. c) Flow cytometry of RAW264.7 cells after treatment of the complete medium (CTRL), H_2O_2 , or after treatment with CeO_2 ($4.99 \mu\text{g mL}^{-1}$), MMT ($50 \mu\text{g mL}^{-1}$), and $\text{CeO}_2@MMT(1:9)$ ($54.99 \mu\text{g mL}^{-1}$) followed by H_2O_2 (1 mM). Intracellular ROS was indicated by DCFH-DA. d–g) Relative levels of IL-1 β , iNOS, CCL2, and IL-6 in lipopolysaccharide-induced RAW264.7 macrophages after indicated treatments. h) Fluorescence images of HT-29 cells cultured on acrylate-based double-sided tape coated Petri dishes, which were further modified with indicated materials (i.e., CTRL, MMT, CeO_2 , and $\text{CeO}_2@MMT(1:9)$). Blue: DAPI, and green: FITC-phalloidin. Scale bar: 20 μm . Data are presented as mean \pm standard error of the mean ($n = 3$). ** $P < 0.01$, comparison between MMT group and $\text{CeO}_2@MMT(1:9)$ group.

topical application, were used to investigate the degree to which $\text{CeO}_2@MMT(1:9)$ protects cells from ROS-induced damage. In the coincubation test, RAW264.7 cells were cultured in a media containing free $\text{CeO}_2@MMT(1:9)$, meaning that any observed anti-ROS effect could originate either extracellularly through contact with the membrane, or intracellularly after phagocytosis. As depicted in Figure 3b, MMT and $\text{CeO}_2@MMT(1:9)$ had almost no cytotoxicity toward HT-29 cells even up to 50 and $54.99 \mu\text{g mL}^{-1}$, respectively. Free CeO_2 NPs also showed good biocompatibility up to $9.98 \mu\text{g mL}^{-1}$, consistent with previous studies.^[17,22] However, Pt, as a highly active nanozyme, showed obvious cytotoxicity at higher concentrations compared with CeO_2 (Figure S13, Supporting Information), which also affirmed the rationale of using nanocerium. To investigate whether $\text{CeO}_2@MMT(1:9)$ could protect cells from ROS-induced damage, a cellular inflammation model was established by treating RAW264.7 cells with H_2O_2 . After H_2O_2 application, an ROS-sensitive

fluorescent dye, 2',7'-dichlorofluorescein diacetate (DCFH-DA), was applied to stain the cells, and the intracellular ROS level was monitored by flow cytometry (Figure 3c).^[16] Free CeO_2 NPs eliminated $\approx 25.88\%$ of intracellular ROS from H_2O_2 -treated RAW264.7 cells while $\text{CeO}_2@MMT(1:9)$ eliminated 73.33% of intracellular ROS as compared to cells treated with H_2O_2 only, demonstrating the nanozyme assembly to have much greater ROS scavenging ability. In contrast, MMT treatment slightly increased intracellular ROS level, which was probably due to the promotion of superoxide anion and hydroxyl radicals by trace metals in MMT.^[21]

To further understand the anti-inflammatory activity of $\text{CeO}_2@MMT(1:9)$, we studied its effect on the levels of several key pro-inflammatory cytokines. Lipopolysaccharide was used to polarize RAW264.7 macrophages to the M1 phenotype with upregulated expression of IL-1 β , iNOS, CCL2, and IL-6 pro-inflammatory cytokines (as measured by real time PCR).

Compared to the untreated control group, both CeO₂@MMT(1:9) and CeO₂ treated cells displayed decreased expression of these pro-inflammatory cytokines during rapid growth and peak population (at 3 and 6 h respectively) (Figure 3d–g). Interestingly, while MMT reduced the levels of IL-1 β and CCL2 after 6 h, it did not significantly affect the expression of IL-6 and even increased the expression of iNOS. The effect of MMT was consistent with the assay data shown in Figures 2e,g, and 3c, which demonstrated that MMT had negligible ROS scavenging activity and even slightly increased ROS production.^[23]

While these results are favorable, we were concerned that traditional cell culture may not fully reflect the nanozyme application to the inflamed colon, where most CeO₂@MMT(1:9) is expected to be adsorbed outside the cells (Figures 3a(2) and 5). To mimic such a situation, we devised a cell culture method to allow prolonged topical application, with CeO₂@MMT(1:9) (or CeO₂, MMT) immobilized onto a Petri dish via acrylate-based double-sided tapes (Figure 3a(2)).^[24] In these modified Petri dishes (Figure S14, Supporting Information), HT-29 cells were seeded onto surfaces coated with the various substrates and evaluated. As shown in Figure 3h and Figure S15, Supporting Information, cytoskeletons were stained with FITC-phalloidin (green) and nuclei were stained with DAPI (blue) after 1- and 3-day culture. Sporadic HT-29 cells were observed in the control group (i.e., acrylate-based double-sided tape), indicating poor adhesion to the highly hydrophobic surface. However, significantly more and larger HT-29 cells were adhered on MMT-, CeO₂-, and CeO₂@MMT(1:9)-modified Petri dishes, due to the better hydrophilicity, rougher surfaces, and the positive charges of ceria. These results demonstrated that the topical application of CeO₂ containing materials exhibited no ill-effect on HT-29 cells proliferation as compared with MMT, and in fact both CeO₂ and CeO₂@MMT(1:9) promoted HT-29 cells proliferation under these conditions. DCF fluorescent imaging of the adhered cultures revealed that CeO₂@MMT(1:9) and CeO₂ also showed significantly lower intracellular ROS levels compared to MMT and controls in these cultures, which was attributed to the significant ROS scavenging activities of CeO₂@MMT(1:9) and CeO₂ (Figure S16, Supporting Information).^[24] Combined, these results demonstrate that CeO₂@MMT(1:9) effectively reduces intracellular ROS levels even without internalization.

2.4. Stability of CeO₂@MMT(1:9) in Digestive Tract

For oral delivery of CeO₂@MMT(1:9) to be viable for IBD therapy, it is critical that the nanoassembly be stable in the stomach and small intestine, especially in the presence of strong acid, which is still a great challenge for most nanomedicines.^[25] Previously, we showed that Mn₃O₄ nanozyme had a better ability to eliminate ROS than CeO₂ nanozyme. However, the stability of Mn₃O₄ nanozyme was poor in simulated gastric juice, which prevented its usage in the current study (Figures S17 and 18, Supporting Information). To investigate the stability of CeO₂@MMT(1:9) in the digestive tract, we examined CeO₂@MMT(1:9) after treating with simulated gastric fluids (SGF, pH = 1.2–1.5, HCl solution) for 4 h at 37 °C corresponding to the maximum human gastric transit time (Figure 4a).^[23] Notably, a hydrogel rapidly formed when a CeO₂@MMT(1:9)

solution (10 mg mL⁻¹, pH \approx 7.0) was mixed with SGF at 37 °C and persisted for the duration (inset of Figure 4a, upper left). Interestingly, when adding NaOH solution (0.1 M) into the CeO₂@MMT hydrogel to adjust pH to about 8.0, the hydrogel was reverted to a homogeneous low viscosity liquid phase (inset of Figure 4a, lower left). This unique phase transition behavior of CeO₂@MMT(1:9) (i.e., hydrogel in low pH gastric juice and liquid phase in high pH intestine) enabled it to maintain its intact structure, and more importantly, ROS-scavenging activity during oral administration.^[26]

Further, we used TEM and XRD to check the structure of CeO₂@MMT(1:9) after treating with SGF. The TEM images showed that CeO₂ NPs were still loaded onto the surface of MMT (Figure 4b), while the XRD results indicated CeO₂@MMT(1:9) retained its crystalline structure after the SGF treatment (Figure S19, Supporting Information). Interestingly, the loading rate of CeO₂ NPs in CeO₂@MMT(1:9) was not significantly changed after treating with SGF (Figure S20a, Supporting Information). To directly verify the stability of CeO₂@MMT(1:9) in the digestive tract of mice, we investigated CeO₂@MMT(1:9) extracted from isolated digestive juice. There were some CeO₂@MMT(1:9)-like materials remained in the gastric juice and intestinal juice (Figure S21, Supporting Information). We also measured the zeta potential of CeO₂@MMT(1:9) in different digestive environment pH. As shown in Figure 4c, the zeta potentials of CeO₂@MMT(1:9) in pH 1.2 (SGF), 7.0 (water), and 8.2 (SCF, simulated colonic fluid) were -22.1 ± 1.7 , -29.0 ± 0.6 , and -30.3 ± 0.3 mV, respectively. These results indicated that CeO₂@MMT(1:9) could retain its negatively charged property when passing through the digestive tract with different pH values.

The ROS scavenging activity after treating with gastric juice is very important for treatment of IBD, so we investigated the remaining ROS scavenging activity of MMT, CeO₂ and CeO₂@MMT(1:9) after treating with SGF. Notably, after SGF treatment, CeO₂@MMT(1:9) retained 75.9% of SOD-like, 79.4% of CAT-like, and 30.3% of \cdot OH scavenging activities (Figure 4d). CeO₂ showed slightly higher ROS-scavenging activities than CeO₂@MMT(1:9), which was due to their better dispersion after treating with HCl solution (Figure 20b–d, Supporting Information). The intact structure, negative charge, and ROS scavenging activity after SGF treatment demonstrated that the postulated targeted adsorption and anti-inflammation therapy of CeO₂@MMT(1:9) would be retained after transit to the inflamed colon.

2.5. CeO₂@MMT(1:9) Preferential Adhesion to Inflamed Mucosa

As discussed, we expect the negative charges of CeO₂@MMT(1:9) to facilitate its adhesion to positively charged inflamed colon epithelia (Figure 5b,c). To verify this hypothesis, we first analyzed the in vitro adhesive properties of CeO₂@MMT(1:9) to polystyrene plates modified with either positively charged amine-rich polymer or negatively charged carboxylate-rich polymer to simulate inflamed and healthy epithelia, respectively (Figure S22, Supporting Information). After incubation of CeO₂@MMT(1:9) on the customized plates for 3 h at 37 °C, the

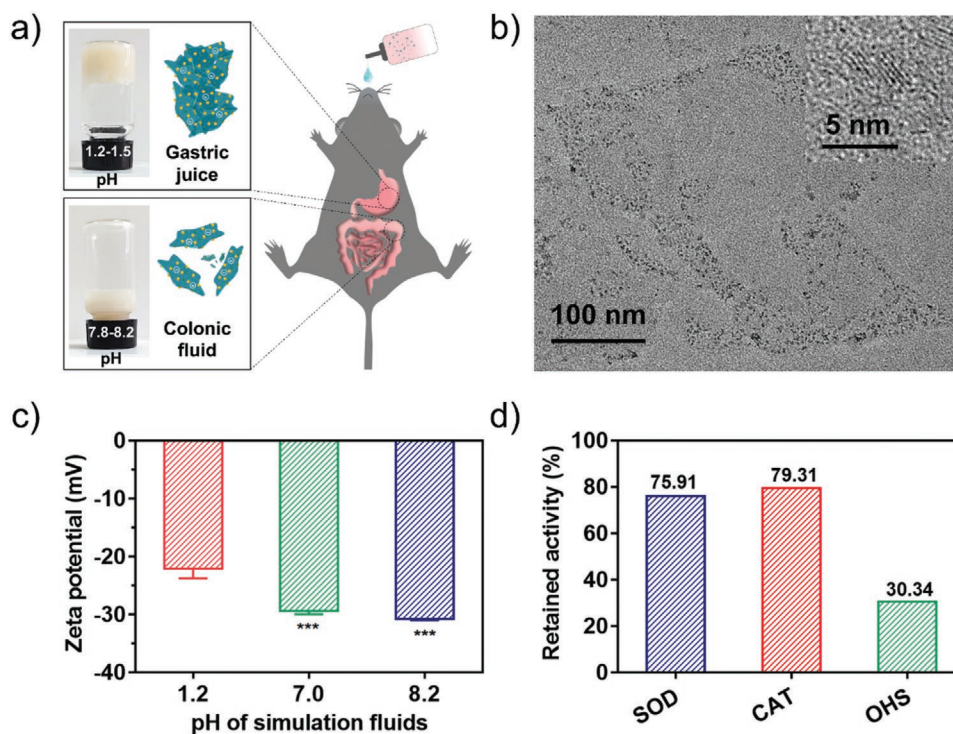


Figure 4. Stability of CeO_2 and $\text{CeO}_2@MMT(1:9)$ in digestive tract mimicking system. a) The process of $\text{CeO}_2@MMT(1:9)$ passing through the digestive tract after oral administration. Inset: photographs of $\text{CeO}_2@MMT(1:9)$ in simulated gastric fluid (i.e., pH = 1.2–1.5 solution) and simulated colonic fluid (i.e., pH = 7.8–8.2 solution). b) TEM image of $\text{CeO}_2@MMT(1:9)$ treated with HCl solution (pH=1.2) for 4 h at 37 °C. c) Zeta potentials of $\text{CeO}_2@MMT(1:9)$ in different simulated gastric fluids (stomach: pH=1.2; colon: pH=8.2). d) Retained ROS-scavenging activities of $\text{CeO}_2@MMT(1:9)$ after treating with gastric juice mimicking solution (i.e., pH = 1.2–1.5 solution). Retained activity = activity after SGF treatment/activity before SGF treatment. SOD-like disproportionation of $\cdot\text{O}_2^-$, CAT-like disproportionation of H_2O_2 , and $\cdot\text{OH}$ scavenging activities (OHS). The measurement methods are the same as in Figure 2e–g. Data are presented as mean \pm standard error of the mean ($n = 3$). *** $P < 0.001$ compared to the group of pH ≈ 1.2 .

absorbed materials were analyzed by using EDS mapping. As shown in Figure 5d–f, and Figure S23, Supporting Information, aminated plates retained a 9.45-fold higher amount of MMT from $\text{CeO}_2@MMT(1:9)$ compared with uncoated plates. The preferential absorption of $\text{CeO}_2@MMT(1:9)$ onto the aminated plates was attributed to the electrostatic interaction between them.

We then examined the ex vivo adhesion of $\text{CeO}_2@MMT(1:9)$ to inflamed colon epithelium by using mice with DSS-induced colitis. Mice were fed with 2% DSS (w/v) every day for 75 consecutive days (day 0 to day 7.5) to induce colitis. On day 6 after DSS induction (Figure 5a and Figure S24, Supporting Information), mice were orally treated with $\text{CeO}_2@MMT(1:9)$ once. 36 h after the treatment, the distal colons of colitis and healthy mice were collected for bio-TEM imaging. The colon tissues were stripped, fixed, and observed by using TEM. Compared with mice fed with H_2O (Figure 5g–h), there was a significant damage to the intestinal tissue of DSS-induced mice as indicated by the abnormal intestinal villi (Figure 5i). Encouragingly, $\text{CeO}_2@MMT(1:9)$ was observed only on the colons from mice with DSS-induced colitis (Figure 5i). No $\text{CeO}_2@MMT(1:9)$ was observed on the healthy colon epithelium (Figure 5h). Together these experiments provided convincing evidence that $\text{CeO}_2@MMT(1:9)$ preferentially adhered to the inflamed colon mucosa via electrostatic interaction.

2.6. Amelioration of Colitis with $\text{CeO}_2@MMT(1:9)$

Based on the excellent ROS scavenging activity, high stability in digestive tract, and inflamed colon targeting capability of $\text{CeO}_2@MMT(1:9)$, the in vivo therapeutic efficacy for the treatment of DSS-induced IBD model in C57BL/6 mice was investigated.^[27] Figure 6a summarizes the overall experimental procedure. Mice were given 2% (w/v) DSS in drinking water for 8 consecutive days to induce colitis. In the early stage of colitis, mice were orally administered $\text{CeO}_2@MMT(1:9)$ on days 5, 7, and 9 (Figure 6a). The therapeutic efficacy was first evaluated by measuring changes in body weight, an important parameter for monitoring the colitis phenotype (Figure 6b). Compared with their initial weight, the body weight of DSS-induced colitis mice decreased by $\approx 16.7\%$ in 9 days. Unfortunately, there were two mouse deaths on days 10 and 11 (red box in Figure 6b), demonstrating the severity of the untreated colitis. As expected, the body weight of healthy mice gradually increased. After therapy for 6 days, the body weight of the colitis mice treated with $\text{CeO}_2@MMT(1:9)$, MMT, and CeO_2 decreased by 4.6%, 10.3%, and 14.6%, respectively. The therapeutic efficacy was also evaluated by measuring the changes in colon lengths and by observing pathological sections. As shown in Figure 6c and Figure S25, Supporting Information, $\text{CeO}_2@MMT(1:9)$ treatment provided mice the best protection against DSS-induced shortening of colon length. As shown in Figure 6d, for the

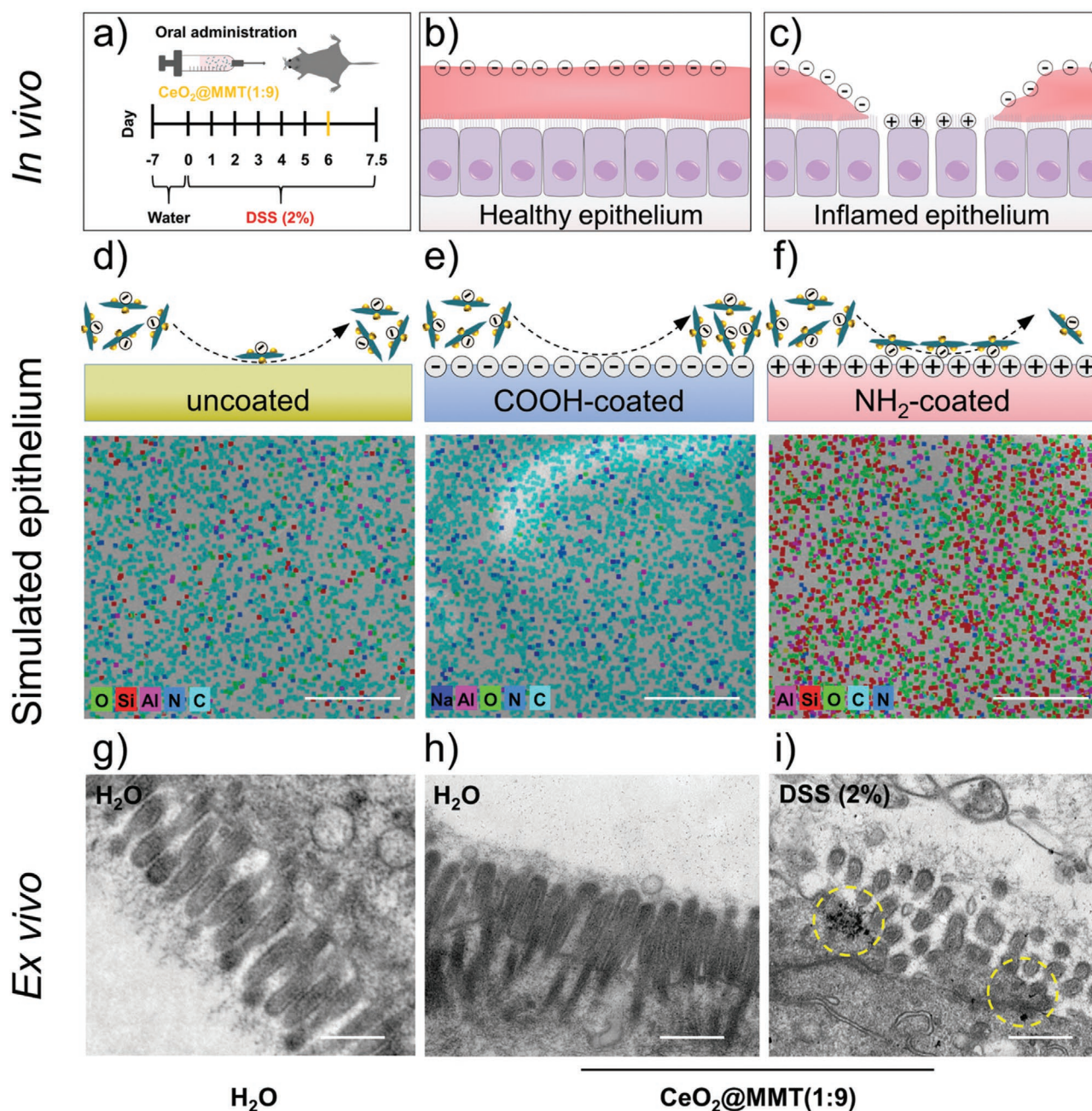


Figure 5. $\text{CeO}_2@\text{MMT}(1:9)$ preferentially adhered to inflamed mucosa. a) Mouse treatment experimental protocol. IBD was induced by treatment with DSS (2%, w/v), once a day for 6 days. On day 6, mice were orally administered with $\text{CeO}_2@\text{MMT}(1:9)$. b,c) Schematic of healthy and inflamed mucosa. The latter is characterized by mucus depletion, accumulation of positively charged proteins, and increased permeability of the epithelial cell layer. d–f) EDS mapping images of $\text{CeO}_2@\text{MMT}(1:9)$ incubated onto uncoated, carboxylate-coated (negatively charged, mimicking healthy epithelium), and ammonium-coated (positively charged, mimicking inflamed epithelium) polystyrene surfaces at 37 °C for 3 h in vitro. Scale bars: 50 μm . g) Bio-TEM image of healthy mouse mucosa. (h,i) Bio-TEM images of healthy and inflamed mouse mucosa at 36 h after treatment with orally administered $\text{CeO}_2@\text{MMT}(1:9)$. $\text{CeO}_2@\text{MMT}(1:9)$ indicated in yellow circles. Scale bars: 500 nm.

DSS-induced colitis mice, the structure of colonic tissue collapsed and the colonic epithelium was disrupted severely. After the treatment, improved histological appearance was observed. Moreover, treatment with $\text{CeO}_2@\text{MMT}(1:9)$ showed the most evident improvement compared with treatments with MMT and CeO_2 . DSS-induced mice also developed symptoms including diarrhea and bloody stools (Figure 6e). Notably,

$\text{CeO}_2@\text{MMT}(1:9)$ significantly inhibited the diarrhea and bloody stools while MMT and CeO_2 partially relieved the symptoms. Moreover, $\text{CeO}_2@\text{MMT}(1:9)$ as well as CeO_2 and MMT exhibited good hemostatic activities, retaining a critical feature of MMT for treatment of intestinal diseases (Figure S26, Supporting Information). These results demonstrated the superior efficacy of $\text{CeO}_2@\text{MMT}(1:9)$ to MMT and CeO_2 for colitis therapy.

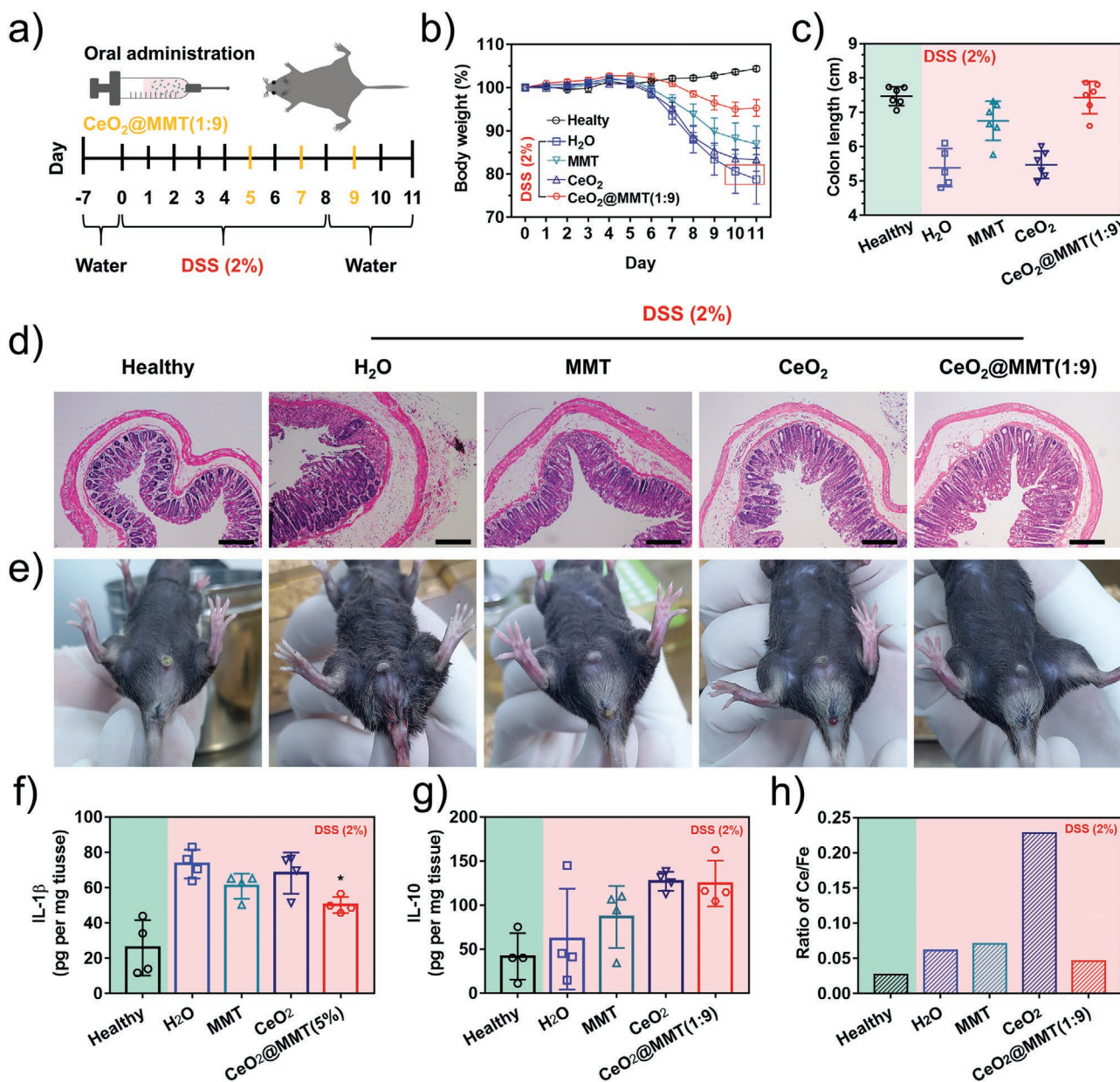


Figure 6. CeO₂@MMT(1:9) therapy in mice with IBD. a) Experimental design of DSS-induced IBD model mice and the timing of treatment (once a day). On days 5, 7, and 9, mice were orally administered H₂O or indicated nanomedicines (indicated by yellow lines). b) Daily body weight over 11 days. The red rectangles indicate mouse deaths on days 10 and 11. c) Colon lengths of mice with indicated treatments on day 11. d) Hematoxylin and eosin stained colonic pathological sections of mice treated with the indicated materials on day 11. Scale bars: 200 μm. e) Representative photographs of rectal areas of a healthy mouse and IBD mice after treatment with H₂O, MMT, CeO₂, and CeO₂@MMT(1:9), respectively (on day 11). f,g) Local concentrations of pro-inflammatory cytokine (IL-1β) and anti-inflammatory cytokine (IL-10) in inflamed colon homogenate. h) Ratio of Ce/Fe from sera of healthy and IBD mice after indicated treatments on day 11. Data are presented as mean ± standard error of the mean (n = 4). *P < 0.05 compared to the H₂O group.

To further understand the therapeutic mechanism of CeO₂@MMT(1:9) toward IBD, the levels of several inflammation-associated cytokines in colon tissues were quantified by using enzyme-linked immunosorbent assay (ELISA). As shown in Figure 6f,g, among the treatment groups, CeO₂@MMT(1:9) treatment significantly reduced the level of pro-inflammatory cytokine IL-1β while increasing the level of anti-inflammatory cytokine IL-10. Additionally, the level of iNOS, a typical M1 type pro-inflammatory factor inversely associated with

anti-inflammation therapy, was evaluated. CeO₂@MMT(1:9) treatment decreased the number of pro-inflammatory iNOS positive monocytes in colitis mice remarkably, as visualized by using immunofluorescence imaging (Figure S27, Supporting Information). Furthermore, the natural enzyme activities of SOD and glutathione peroxidase (GPx), two representative anti-inflammation enzymes, in sera from healthy and IBD mice after treatments were assessed (Figure S28, Supporting Information). Interestingly, CeO₂@MMT(1:9) treatment increased

SOD activity but decreased GPx activity. Combined the in vitro (Figure 2d–g) and in vivo results (Figure 6f,g and Figure S27, Supporting Information) suggest that the reduction in ROS due to the presence of CeO₂@MMT(1:9) promoted recovery of inflamed colon tissue by decreasing pro-inflammatory cytokines and increasing anti-inflammatory cytokines.

Finally, the in vivo biocompatibility of CeO₂@MMT(1:9) was studied. Since orally administered nanomedicines usually suffer from systemic absorption, the serum levels of Ce were determined to evaluate the safety of CeO₂@MMT(1:9). As shown by the ratios of Ce/Fe for mice in each treatment group in Figure 6h and Figure S29, Supporting Information, the systemic absorption of CeO₂@MMT(1:9) was significantly minimized compared with free CeO₂ NPs, demonstrating the advantage of our design. Additionally, there was no obvious histological abnormality of heart, liver, spleen, lung, or kidney of colitis mice after therapy, suggesting CeO₂@MMT(1:9) as well as CeO₂ and MMT possessed good histocompatibility (Figure S30, Supporting Information). Such an excellent biocompatibility of CeO₂@MMT(1:9) could be attributed to its targeting capability as well as the intrinsic biocompatibility of CeO₂ and MMT.

2.7. Preliminary Evaluation of Translational Promise of CeO₂@MMT

To further demonstrate the translational promise of our nanozyme, a clinically approved MMT (MMT(A)) was used to fabricate CeO₂@MMT(A) by using it as the substrate for in situ growth of CeO₂ NPs. Structural characterization showed that CeO₂@MMT(A) exhibited very similar morphology, crystallinity, and loading of CeO₂ NPs, as compared with CeO₂@MMT(1:9) (Figures S31, S32, and S33, Supporting Information). Encouragingly, the CeO₂@MMT(A) also had an excellent CAT-like activity (Figure S34, Supporting Information). Combined with the good biocompatibility of CeO₂@MMT, this result indicated the use of clinically available MMT should facilitate rapid translation of the CeO₂@MMT into clinic.

3. Discussion

The conventional treatment of IBD, a refractory chronic disease, suffers from limited efficacy and systemic side-effects, partially due to the lack of effective targeted therapies.^[28] Recently developed nanomedicines have provided several novel strategies to specifically target diseased colon. Hyaluronic acid (HA)–bilirubin nanoparticles were shown to accumulate and eliminate inflammation in the inflamed mucosa of colitis mice owing to the interaction of HA with surface protein CD44.^[7b] Antibody-coated poly(lactic acid) particles were designed to target inflamed intestine owing to the specific interaction between antibodies and upregulated endothelial receptors.^[29] A negatively charged hydrogel, consisting of ascorbic acid and palmitic acid, was used to load dexamethasone for targeting inflamed mucosa via the electrostatic interaction between the hydrogel and inflamed colon epithelium.^[6a] While these treatments demonstrated success in remediating the disease state,

they each have limitations. Some used stoichiometric anti-oxidants, which were consumed as they eliminated ROS, thus requiring repeated dosing of large amounts of active agent, while others employed enema for administration, which is not patient-friendly.

By exploring the pathological characteristics of inflamed colon as well as the unique physicochemical properties of MMT and CeO₂, here, we designed an orally administered CeO₂@MMT(1:9) nanozyme for targeted colitis therapy. We demonstrated that the negatively charged CeO₂@MMT adheres preferentially to positively charged surfaces, and in vivo localizes to the positively charged inflamed mucosa in murine colitis subjects. Importantly, both in vitro digestive tract simulation results and ex vivo animal studies showed that CeO₂@MMT(1:9) possessed a stable structure with smart phase response to pH, negative charges, and ROS scavenging activities. These features enabled CeO₂@MMT(1:9) to be efficiently delivered through the digestive tract via orally administration, and specifically target the inflamed colon and alleviate inflammation. Unexpectedly, CeO₂@MMT(1:9) remained adsorbed on the intestinal wall of colitis mice 36 h after administration. This persistent targeting could increase the effectiveness of the drug, thereby reducing the administration frequency and dose. On the other hand, CeO₂@MMT(1:9) still retained the intrinsic therapeutic properties of MMT, such as reduced bleeding and tissue protection.^[13b] Moreover, the growth of CeO₂ NPs onto MMT minimized its systemic absorption and thus reduced potential toxicity.^[11]

Importantly, the mechanism of action of CeO₂ NPs is different than that of small molecule antioxidant pharmaceuticals; while these can only act stoichiometrically, CeO₂ NPs act catalytically to scavenge excess ROS to reduce inflammation in colitis affected colon meaning that substantially less material need be administered. As a high performance nanozyme, nanoceria exhibited not only SOD- and CAT-like activities but also •OH scavenging activity. In contrast, there is no corresponding enzymes in live organisms to scavenge •OH.^[20] Compared with enzyme-based therapeutics, nanoceria showed several advantages, such as excellent stability, multi-enzyme activity, and minimal immunogenicity. Consequently, when used for IBD therapy, CeO₂@MMT(1:9) showed excellent efficacy. Notably, CeO₂@MMT(1:9) regulated the local immunological environments of lesion tissues by significantly downregulating pro-inflammatory cytokines level and simultaneously upregulating anti-inflammatory cytokine levels.

4. Conclusions

In conclusion, this work demonstrated a novel nanozyme medicine to specifically target inflamed colon and effectively scavenge excessive ROS via oral administration. By combining the complementary features of each individual component (i.e., CeO₂ and MMT), the designed CeO₂@MMT with multifaceted therapeutic properties significantly improved the colitis model of mice. Given the fast development of nanozymes,^[30] other ROS scavenging nanozymes are expected to be combined with MMT for IBD therapy. MMT as well as other clay minerals could be further investigated as potential carriers. Furthermore, ROS scavenging nanozymes could be conjugated with other

targeting moieties for anti-inflammation therapies. In addition, the high therapeutic efficacy and significantly minimized systemic toxicity of our nanozyme, which is still the greatest concern of nanomedicine (Figure S35, Supporting Information), will inspire novel strategies for future nanomedicine.

5. Experimental Section

Materials: Cerium nitrate hexahydrate (99.95%), ethylene glycol (AR, 98%), and ammonia solution (AR, 25–28%) were obtained from Aladdin (Shanghai, China). MMT were obtained from Nanocor (Nanometer, PGW, USA). All other reagents and chemicals were purchased from commercial sources and used as received.

Material Characterization: The size, morphological, structural, and element distribution studies were carried out by using a FEI TECNAI F20 TEM at an acceleration voltage of 200 kV and a Quanta 200 SEM (Quanta 200) at an acceleration voltage of 10 kV. All the XRD spectra were recorded by using Rigaku Ultima diffractometer with 2° min^{-1} using Cu K α radiation. XPS measurements were carried out by using a Thermo Scientific K-Alpha spectrometer, of which an Al K α (1486 eV) anode and a hemispherical energy analyzer were used. The binding energy was calibrated by using a contaminant carbon (C1s = 284.6 eV), and the binding energy of the Ce 3d states of the ceria for analysis were in Table S1, Supporting Information. The zeta potentials were measured at 25 °C in water or simulation fluids by using a Malvern Zetasizer Nano ZSP instrument equipped with a Malvern surface zeta potential cell. The concentrations of ceria contained in all the samples were determined by using an inductively coupled plasma optical emission spectrometer (PerkinElmer's Avio 500).

Preparation of CeO₂@MMT and CeO₂: CeO₂@MMT was prepared as follows. First, 2 and 5 g MMT powders were added to 100 mL of water under vigorous stirring for 48 h to form uniformly dispersed MMT suspensions with concentrations of ≈ 20 and 50 mg mL⁻¹, respectively. Then 10 mL of ethylene glycol solution containing 126 mg Ce(NO₃)₃·6H₂O was added into 10 mL of the prepared MMT suspension dropwise under vigorous stirring over 5 min. The above solution was then put into a water bath at 60 °C for further vigorous stirring. After 10 min, 1.6 mL of ammonia water (28–30%) was quickly injected into the mixed solution by a syringe. After 3 h, the formed CeO₂@MMT were collected by centrifugation and washed thoroughly with water until the pH of the filtrate solution was neutral. Finally, the products were re-dispersed in water or lyophilized for further use. Note, the two products were denoted as CeO₂@MMT(2:8) and CeO₂@MMT(1:9) according to the ratio (w/w) of ceria to MMT in CeO₂@MMT (Figure S3, Supporting Information). Free ceria NPs were prepared by using the same method for the synthesis of CeO₂@MMT, without the addition of MMT. Note, the free ceria NPs were denoted as CeO₂ (for the simplicity, the oxygen vacancy was not shown in both CeO₂@MMT and CeO₂).

SOD-Like Activity Measurements: The SOD-like activities of CeO₂ and CeO₂@MMT were assessed by using a SOD assay kit (Dojindo, Japan). First, 20 μL of each material with a final concentration in ceria (20 $\mu\text{g mL}^{-1}$) was mixed with 200 μL of a 2-(4-iodophenyl)-3-(4-nitrophenyl)-5-(2,4-disulphophenyl)-2H tetrazolium sodium salt working solution in a microplate well. Then, 20 μL of the enzyme working solution was added. After incubation at 37 °C for 20 min, the absorbance at 450 nm was measured by using a multiple plate reader (Tecan Infinite 200 Pro). The elimination rate of the superoxide was calculated by measuring the decrease in color development. MMT(8) and MMT(9) with an equal amount of MMT to CeO₂@MMT(2:8) and CeO₂@MMT(1:9), respectively, were used as the control samples to examine the effect of MMT. The accuracy was assessed by the replicate analysis ($n = 3$).

CAT-Like Activity Measurements: The CAT-like activities of CeO₂ and CeO₂@MMT were assessed by measuring the amount of generated oxygen with a dissolved oxygen meter (SevenExcellence Multiparameter, Mettler Toledo Co., Ltd.). Briefly, each material and H₂O₂ were successively added into 6 mL of water. CeO₂, MMT, CeO₂@MMT(2:8),

and CeO₂@MMT(1:9) had a final concentration in ceria of 100 $\mu\text{g mL}^{-1}$. The final concentration of H₂O₂ was 5 mM. After incubation for 30 min at room temperature, the reaction solution was centrifuged to remove the material, which minimized the potential interference of materials. Then, the amount of generated oxygen (mg L⁻¹) was detected. MMT(8) and MMT(9) with an equal amount of MMT to CeO₂@MMT(2:8) and CeO₂@MMT(1:9), respectively, were used as the control samples to examine the effect of MMT. The accuracy was assessed by the replicate analysis ($n = 3$).

Hydroxyl Radical Scavenging Activity^[6]: The hydroxyl radical scavenging activities of CeO₂ and CeO₂@MMT were assessed by using EPR analysis, performed on a Bruker EMX10/12 spectrometer with X-band capabilities. The $\cdot\text{OH}$ was trapped by DMPO in aqueous solution by forming spin adduct DMPO/OH. $\cdot\text{OH}$ was generated using Fenton reaction and the ESR signals were obtained by mixing 25 mM BMPO, 1.0 mM FeSO₄ and 1.0 mM H₂O₂ in water. In $\cdot\text{OH}$ scavenging activity experiment, EPR spectra of DMPO/OH were recorded at 90 s past incubation of newly generated $\cdot\text{OH}$, DMPO and samples. CeO₂, CeO₂@MMT(2:8), and CeO₂@MMT(1:9) had an equal concentration of ceria (20 $\mu\text{g mL}^{-1}$), meanwhile, MMT(8) and MMT(9) with an equal amount of MMT to CeO₂@MMT(2:8) and CeO₂@MMT(1:9), respectively, were used as the control samples to examine the effect of MMT. Because the typical EPR spectrum of DMPO/OH reveals four lines with relative intensities of 1:2:2:1, so the second line's intensity was used to calculate the elimination rate of samples. The accuracy was assessed by the replicate analysis ($n = 3$).

Cell Culture: RAW264.7 cells and HT-29 colonic epithelial cell lines were obtained from the Cell Bank of the Chinese Academy of Sciences (Shanghai, China). RAW264.7 cells and HT-29 cells were cultured in high glucose-DMEM medium (Gibco, USA) containing 5% or 10% (v/v) FBS, 1% penicillin/streptomycin in a humidified 5% CO₂ atmosphere at 37 °C.

Cell Viability: HT-29 cells were seeded at 5×10^3 cells per well in 96-well plates. After 1 day, the different concentrations of materials were added to the cells. Cell viability was quantified after 24 h of incubation using CCK-8 (Dojindo Laboratories, Japan) according to manufacturer's instructions by a microplate reader (Tecan Infinite 200 Pro). Data are means \pm SD ($n = 4$).

The viability of cells was calculated using the equation

$$\text{Viability} = \frac{O_t}{O_c} \times 100\% \quad (1)$$

where O_t is the absorbance of the testing samples and O_c is the absorbance of the control groups.

ROS Scavenging Ability of RAW264.7 Cells: First, RAW264.7 cells with a density of 5×10^5 cell mL⁻¹ were cultured on the surfaces of all samples in 6-well culture plates for 12 h. Then new standard growth medium containing different concentration of materials was added and further incubated for 4 h. Next a fresh medium containing 1 mM H₂O₂ was used to stimulate all groups for 3 h except the negative group. Last flow cytometry of RAW264.7 cells were used to detect the ROS scavenging ability.

Flow Cytometry: After stimulating, the RAW264.7 cells were incubated with DCFH-DA (Beyotime Biotechnology, China) for 20 min, then washed with PBS for three times, collected by centrifugation and analyzed by flow cytometry using the FL1 flow cytometer detection channels (ACEA NovoCyte). The excitation wavelength was 488 nm and the emission wavelength was 525 nm.

Analysis of Effect of CeO₂@MMT(1:9) on Cells after Topical Application: In order to investigate the effect of CeO₂@MMT(1:9) on inflamed cells when they were absorbed outside the colonic epithelial cells, HT-29 cells were seeded onto various modified Petri dishes and analyzed as shown in Figure 3a(2): First, CeO₂, MMT and CeO₂@MMT(1:9) powders were ground into a fine powder. Then, one surface of 3M double-sided tapes (3M) was used to adhere powders, while the other surface of tapes was adhered on the glasses as a supporting. All prepared samples were pressed under heavy objects to ensure a long-lasting adhesion. After 12 h, the non-adhered materials on the surfaces were cleaned by sonication for 2 min, subsequently all samples were cleaned with water five times.

Before cells inoculation, the material adhered 3M tapes were sterilized by incubation into 75% (v/v) ethanol for 30 min. After sterilization, 3M, MMT-3M, CeO₂-3M, and CeO₂@MMT(1:9)-3M surfaces were placed in DMEM medium to remove the residual ethanol. After cleaning, HT-29 cell with a density of 5 × 10⁴ cell mL⁻¹ were seeded on the above four surfaces and cultured in 24-well culture plates for 1 and 3 days.

Adhesion and Viability of HT-29 Cells: The morphologies of actin cytoskeleton of cells were investigated on day 1 and day 3. Briefly, cells were washed with PBS, fixed with 4% paraformaldehyde (Sangon, China), permeabilized with 0.1% Triton (Sigma, USA), and blocked in 1 wt% bovine serum protein (BSA; CST, USA). F-actins were stained with FITC phalloidin (Cytoskeleton, USA) at 37 °C in the dark for 1 h. Nuclei were stained with DAPI (SouthernBiotech, USA). All the cells were observed by using a fluorescence microscope (Axio Observer A1, Zeiss, Germany).

ROS Scavenging Ability: First, HT-29 cells with a density of 5 × 10⁴ cell mL⁻¹ were cultured on the four surfaces in 6-well culture plates for 1 day, then using new standard growth medium containing 5 mM H₂O₂ to stimulate samples for 1 day. After the pretreatment and H₂O₂ stimulating, all cells were washed with α-MEM lacking phenol red and then incubated in the dark for 10 min in Krebs-Ringer solution containing 5 μM DCFH-DA. Culture dishes were transferred to the Axio Observer A1 inverted microscope (Zeiss, Germany), and DCF (2',7'-dichlorofluorescein) fluorescence was measured with an excitation wavelength of 488 nm and emission at 515–540 nm at the same exposure time.^[31]

Quantitative Reverse Transcription PCR: RAW264.7 cells (1 × 10⁵) were seeded in a 6-wells plate containing 2 mL cell culture medium and incubated for 12 h. The cells were incubated with CeO₂ (4.99 μg mL⁻¹), MMT (50 μg mL⁻¹), and CeO₂@MMT(1:9) (54.99 μg mL⁻¹) dispersed in completed DMEM media for 4 h incubation. The cells were then washed with PBS for three times and stimulated with 20 ng mL⁻¹ for 3 and 6 h.^[32] Then total RNA was extracted from the RAW264.7 cells using Trizol (Invitrogen Life Technologies, Carlsbad, USA) according to instructions provided by the manufacturer. RNA quality was determined by measuring the optical density at the ratio of 260 and 280 nm. 1.0 μg of total RNA was reverse-transcribed to cDNA. Real time-PCR analysis for IL-1β, iNOS, CCL2, and IL-6 mRNA was performed on a Roche LightCycler 480 Real-Time PCR System (Roche, Switzerland) with ChamQ SYBR Color qPCR Master Mix (Vazyme, Nanjing, China). The primers used for quantitative real-time PCR (Q-PCR) were listed in (Table S2, Supporting Information): IL-1β, iNOS, CCL2, and IL-6 and β-actin. The following Q-PCR conditions were used: 40 cycles of denaturation at 95 °C for 10 s, annealing at 60 °C for 30 s. A comparative threshold cycle method was used to analyze the Q-PCR data, where the amount of target was normalized to the endogenous reference of β-actin in each sample.

Stability Investigation of CeO₂@MMT(1:9) in Simulated Gastric Juice: The stability of CeO₂@MMT(1:9) was evaluated as follows. First, to simulate the digestion process of food in the stomach, 200 mg of CeO₂, MMT, or CeO₂@MMT(1:9) were added into 10 mL of hydrochloric acid solution (as a gastric fluid simulating fluid, pH at 1.2 to 1.5) and incubated at 37 °C with 65 rpm shaking for 4 h.^[25] Then, CeO₂, MMT, or CeO₂@MMT(1:9) were neutralized by washing with water and NaOH solution (0.1 mM). Finally, the materials were dissolved in water or lyophilized for TEM, XRD, ICP, zeta potential measurements, and analysis of ROS scavenging activities. Subsequently, TEM, XRD, and ICP were used to investigate the structural stability of CeO₂@MMT(1:9) before and after treatment with SGF. The zeta potential of materials was used to study the surface charges. Meanwhile, the same mass concentrations of materials were used to examine the retained ROS scavenging activities.

Targeting Simulation of CeO₂@MMT(1:9) In Vitro and Ex Vivo: Based on the changes from negative charges to positive charges on the colon epithelium before and after enteritis, an experiment was designed to investigate the targeting ability of CeO₂@MMT(1:9) to lesion colonic epithelium in vitro. First, polystyrene plates were modified with amine-rich polymer name (positively charged) and carboxylate-rich polymer name (negatively charged) to simulate inflamed and healthy epithelia,

respectively. Then, the modified surfaces were stained using acid orange and toluidine blue solutions to confirm the successful modification of carboxyl- and amino-groups, respectively. The modified surfaces were named as carboxyl-group and amino-group while the pristine surface with neutral charges was named as uncoated surface. Third step, the three modified polystyrene plates were incubated in 5 mg mL⁻¹ of CeO₂@MMT(1:9) solution at 37 °C for 3 h, subsequently using water (Requires gentle operation) to wash out CeO₂@MMT(1:9) that was physically deposited on the surfaces. At last, EDS mapping and spectra were used to detect the content of CeO₂@MMT(1:9) sheets on the different surfaces.

Bio-TEM imaging was used to further demonstrate the targeting ability of CeO₂@MMT(1:9) to lesion colonic epithelium in vivo. Briefly, male C57BL/6 mice were received 2% (w/v) DSS to the sixth day, then 55 mg kg⁻¹ of CeO₂@MMT(1:9) was administered via an oral route into DSS or healthy mice (Figure 5a). After 36 h mice were sacrificed, the colons without feces were fixed with 4% paraformaldehyde, then the biological samples were prepared for TEM imaging.

Animal Studies: The anesthetic, surgical, and post-operative care protocols were examined and approved by the Animal Ethics Committee of Nanjing Drum Tower Hospital and conducted under the Institutional Committee of Care and Use of Laboratory Animals. 6-week-old male C57BL/6 mice weighing ≈25 g from the Experimental Animal Center of Nanjing Medical University were used in this study.

DSS-Induced Model of Colitis^[27]: 6-week-old male C57BL/6 mice were housed in groups of seven mice per cage and acclimatized for 1 week before inclusion in the study. Mice received 2% (w/v) DSS (40 kDa; Dalian Meilun Biotechnology Co., China) supplemented in the drinking water (sterilized) for 8 days, followed by normal water. Control healthy mice were provided with normal water only. Then 50 mg kg⁻¹ of MMT, 5 mg kg⁻¹ of CeO₂, 55 mg kg⁻¹ of CeO₂@MMT(1:9) or water was administered via an oral route into mice on predetermined days (Figure 6a). Changes in bodyweight were assessed daily over the 11-day experimental period. On the last day of the experiment, mice were sacrificed and the entire colon and organs were excised. Colon length was measured and gently washed with physiological saline. Then, two pieces of the distal sections (0.5 cm in length) were used for histological assessment and immunofluorescence staining. The remaining colon tissue samples were used for the evaluations of cytokines.

Histological Analysis: For histological analyses, hematoxylin and eosin stained colonic tissue sections were prepared. Briefly, centered at the lesion site, 1.0 cm section of the distal colon was separated, post-fixed by 4% paraformaldehyde for 6 h and then embedded in paraffin. Longitudinal or transverse sections (5 μm thick) were mounted on slides for subsequent staining.

ELISA Analysis: For pro-inflammatory and anti-inflammatory cytokines evaluation, the amount of IL-1β and IL-10 in colon homogenate was quantified by ELISA test. The middle colon of each mouse was weighed and homogenized in 4 °C saline. Then, the resultant homogenate was centrifuged at 2000 rpm for 20 min at 4 °C, and the supernatant was collected for evaluation. Commercial mouse IL-1β and IL-10 ELISA Kit (Neobioscience, China) was utilized for the determination of pro-inflammatory and anti-inflammatory cytokines of colon homogenate. To exclude the accidental death of mice in the untreated group, 4 samples of each group were used for quantitative analysis. Data were means ± SD (n = 4).

Ex Vivo Immunofluorescence Imaging: To examine the changes of mice to regulate colon inflammation after treatment with different materials, colons of mice were resected after euthanasia and post-fixed by 4% paraformaldehyde for 6 h and then embedded in paraffin. Longitudinal or transverse sections (5 μm thick) were mounted on slides. Before antibody incubation, all samples were dewaxed with gradient alcohol. Then, samples were permeabilized with 0.1% or 0.25% Triton X-100 and blocked with phosphate buffered saline with Tween 20 (PBST) containing 1% (or 3%) BSA and 22.52 mg mL⁻¹ of glycine. The sections were stained with 1 μg mL⁻¹ of Rabbit Anti-iNOS antibody (Abcam, ab3523) for 1 h followed by 2 μg mL⁻¹ of anti-rabbit secondary antibody conjugated with

AlexaFluor-488 and 5 $\mu\text{g mL}^{-1}$ of Mouse Anti-arginase I(E-2) antibody (Santa Cruz, sc-271430) conjugated with AlexaFluor-488. All fluorescent and phase contrast images were obtained by using an Axio Observer A1 inverted microscope (Zeiss, Germany).

Statistical Analysis: The statistical significance of differences between groups was determined by using one-way ANOVA followed by Tukey post-hoc analysis. Significance was established by a value of $P < 0.05$. Statistical analysis was performed with GraphPad Prism 6.

Data Availability

The data that support the findings of this study are available from the corresponding author upon reasonable request.

Supporting Information

Supporting Information is available from the Wiley Online Library or from the author.

Acknowledgements

This work was supported by National Natural Science Foundation of China (21722503 and 21874067), Natural Science Foundation of Jiangsu Province (BK20180340), the National Key R&D Program of China (2019YFA0709200), PAPD Program, Open Funds of the State Key Laboratory of Analytical Chemistry for Life Science (SKLACLS1704), Open Funds of the State Key Laboratory of Coordination Chemistry (SKLCC1819), and Fundamental Research Funds for the Central Universities (021314380145).

Conflict of Interest

Patents application is in progress.

Author Contributions

H.W. and S.Z. designed the experiments. S.Z. prepared the materials, performed the structural characterization, stability measurements, and analyzed the data. S.Z. and Y.L. completed in vitro biological experiments and analyzed the data. Y.C., Q.L., and C.C. assisted with animal experiment and ex vivo ELISA analysis. Z.S. carried out ex vivo immunofluorescence imaging measurements. S.L. contributed to SEM characterization and enzyme-like activity tests. S.Z., C.B., and H.W. wrote the manuscript with inputs from all the authors.

Keywords

IBD therapies, inflammatory bowel disease, nanoceria, nanozymes, ROS scavengers

Received: June 2, 2020

Revised: August 4, 2020

Published online: September 13, 2020

[1] GBD 2017 Inflammatory Bowel Disease Collaborators, *Lancet Gastroenterol. Hepatol.* **2020**, 5, 17.

[2] M. L. Hoivik, B. Moum, I. C. Solberg, M. Cvancarova, O. Hoie, M. H. Vatn, T. Bernklev, I. S. Group, *Inflammatory Bowel Dis.* **2012**, 18, 1540.

- [3] C. N. Bernstein, M. Fried, J. H. Krabshuis, H. Cohen, R. Eliakim, S. Fedail, R. Geary, K. L. Goh, S. Hamid, A. G. Khan, A. W. LeMair, Malfertheiner, Q. Ouyang, J. F. Rey, A. Sood, F. Steinwurz, O. O. Thomsen, A. Thomson, G. Watermeyer, *Inflammatory Bowel Dis.* **2010**, 16, 112.
- [4] a) A. Stallmach, S. Hagel, T. Bruns, *Best. Pract. Res., Clin. Gastroenterol.* **2010**, 24, 167; b) D. S. Wilson, G. Dalmasso, L. Wang, S. V. Sitaraman, D. Merlin, N. Murthy, *Nat. Mater.* **2010**, 9, 923; c) N. Sela-Passwell, R. Kikkeri, O. Dym, H. Rozenberg, R. Margalit, R. Arad-Yellin, M. Eisenstein, O. Brenner, T. Shoham, T. Danon, A. Shazer, I. Sagi, *Nat. Med.* **2012**, 18, 143.
- [5] C. Lautenschläger, C. Schmidt, D. Fischer, A. Stallmach, *Adv. Drug. Delivery Rev.* **2014**, 71, 58.
- [6] a) S. Zhang, J. Ermann, M. D. Succi, A. Zhou, M. J. Hamilton, B. Cao, J. R. Korzenik, J. N. Glickman, P. K. Vemula, L. H. Glimcher, G. Traverso, R. Langer, J. M. Karp, *Sci. Transl. Med.* **2015**, 7, 300ra128; b) B. C. Dickinson, C. J. Chang, *Nat. Chem. Biol.* **2011**, 7, 504; c) G. Canny, O. Levy, G. T. Furuta, S. Narravula-Alipati, R. B. Sisson, C. N. Serhan, S. P. Colgan, *Proc. Natl. Acad. Sci. U. S. A.* **2002**, 99, 3902; d) M. B. Grisham, *Lancet* **1994**, 344, 859.
- [7] a) T. T. Jubeh, M. Nadler-Milbauer, Y. Barenholz, A. Rubinstein, *J. Drug Targeting* **2006**, 14, 155; b) Y. Lee, K. Sugihara, M. G. Gilliland, S. Jon, N. Kamada, J. J. Moon, *Nat. Mater.* **2019**, 19, 118.
- [8] W. Han, A. Mercenier, A. Ait-Belgnaoui, S. Pavan, F. Lamine, I. I. van Swam, M. Kleerebezem, C. Salvador-Cartier, M. Hisbergues, L. Bueno, V. Theodorou, J. Fioramonti, *Inflammatory Bowel Dis.* **2006**, 12, 1044.
- [9] Q. Zhang, H. Tao, Y. Lin, Y. Hu, H. An, D. Zhang, S. Feng, H. Hu, R. Wang, X. Li, J. Zhang, *Biomaterials* **2016**, 105, 206.
- [10] a) J. Chen, S. Patil, S. Seal, J. F. McGinnis, *Nat. Nanotechnol.* **2006**, 1, 142; b) C. Xu, X. Qu, *NPG Asia Mater.* **2014**, 6, e90; c) J. Wu, X. Wang, Q. Wang, Z. Lou, S. Li, Y. Zhu, L. Qin, H. Wei, *Chem. Soc. Rev.* **2019**, 48, 1004; d) Y. Li, X. He, J.-J. Yin, Y. Ma, P. Zhang, J. Li, Y. Ding, J. Zhang, Y. Zhao, Z. Chai, Z. Zhang, *Angew. Chem., Int. Ed.* **2015**, 54, 1832.
- [11] J. Wang, G. Zhou, C. Chen, H. Yu, T. Wang, Y. Ma, G. Jia, Y. Gao, B. Li, J. Sun, Y. Li, F. Jiao, Y. Zhao, *Toxicol. Lett.* **2007**, 168, 176.
- [12] a) H. B. Yao, Z. H. Tan, H. Y. Fang, S. H. Yu, *Angew. Chem., Int. Ed.* **2010**, 49, 10127; b) S. Jayrajsinh, G. Shankar, Y. K. Agrawal, L. Bakre, *J. Drug Delivery Sci. Technol.* **2017**, 39, 200.
- [13] a) <http://www.cde.org.cn/news.do?method=largeInfo&id=314805> (accessed: March 2020); b) C. Dupont, B. Vernisse, *Pediatr. Drugs* **2009**, 11, 89.
- [14] K. G. Bhattacharyya, S. S. Gupta, *Adv. Colloid Interface Sci.* **2008**, 140, 114.
- [15] B. Li, T. Gu, T. Ming, J. Wang, P. Wang, J. Wang, J. C. Yu, *ACS Nano* **2014**, 8, 8152.
- [16] F. Zeng, Y. Wu, X. Li, X. Ge, Q. Guo, X. Lou, Z. Cao, B. Hu, N. J. Long, Y. Mao, C. Li, *Angew. Chem., Int. Ed.* **2018**, 57, 5808.
- [17] M. Soh, D.-W. Kang, H.-G. Jeong, D. Kim, D. Y. Kim, W. Yang, C. Song, S. Baik, I.-Y. Choi, S.-K. Ki, H. J. Kwon, T. Kim, C. K. Kim, S.-H. Lee, T. Hyeon, *Angew. Chem., Int. Ed.* **2017**, 56, 11399.
- [18] J. Paier, C. Penschke, J. Sauer, *Chem. Rev.* **2013**, 113, 3949.
- [19] S. Melov, J. Ravenscroft, S. Malik, M. S. Gill, D. W. Walker, P. E. Clayton, D. C. Wallace, B. Malfroy, S. R. Doctrow, G. J. Lithgow, *Science* **2000**, 289, 1567.
- [20] P. Dandona, K. Thusu, S. Cook, B. Snyder, J. Makowski, D. Armstrong, T. Nicotera, *Lancet* **1996**, 347, 444.
- [21] D. Vantelon, M. Pelletier, L. Michot, O. Barres, F. Thomas, *Clay Miner* **2001**, 36, 369.
- [22] S. S. Lee, W. Song, M. Cho, H. L. Puppala, P. Nguyen, H. Zhu, L. Segatori, V. L. Colvin, *ACS Nano* **2013**, 7, 9693.
- [23] M. Baek, J.-A. Lee, S.-J. Choi, *Mol. Cell. Toxicol.* **2012**, 8, 95.
- [24] J. Li, J. Wen, B. Li, W. Li, W. Qiao, J. Shen, W. Jin, X. Jiang, K. W. K. Yeung, P. K. Chu, *Adv. Sci.* **2018**, 5, 1700678.

- [25] X. Wang, J.-J. Yan, L. Wang, D. Pan, R. Yang, Y. Xu, J. Sheng, Q. Huang, H. Zhao, M. Yang, *Chem. Mater.* **2018**, *30*, 4073.
- [26] M. Benna, N. Kbir-Arighuib, A. Magnin, F. Bergaya, *J. Colloid Interface Sci.* **1999**, *218*, 442.
- [27] S. Wirtz, C. Neufert, B. Weigmann, M. F. Neurath, *Nat. Protoc.* **2007**, *2*, 541.
- [28] A. Dahan, G. L. Amidon, E. M. Zimmermann, *Expert Rev. Clin. Immunol.* **2010**, *6*, 543.
- [29] H. S. Sakhalkar, M. K. Dalal, A. K. Salem, R. Ansari, J. Fu, M. F. Kiani, D. T. Kurjiaka, J. Hanes, K. M. Shakesheff, D. J. Goetz, *Proc. Natl. Acad. Sci. U. S. A* **2003**, *100*, 15895.
- [30] a) R. W. Tarnuzzer, J. Colon, S. Patil, S. Seal, *Nano Lett* **2005**, *5*, 2573; b) B. Liu, Z. Sun, P.-J. Huang, J. Liu, *J. Am. Chem. Soc.* **2015**, *137*, 1290; c) S. Neri, S. Garcia Martin, C. Pezzato, L. J. Prins, *J. Am. Chem. Soc.* **2017**, *139*, 1794; d) L. Huang, J. Chen, L. Gan, J. Wang, S. Dong, *Sci. Adv.* **2019**, *5*, eaav5490; e) D. Kim, H. J. Kwon, T. Hyeon, *Adv. Mater.* **2019**, *31*, 1807965; f) L. Gao, J. Zhuang, L. Nie, J. Zhang, Y. Zhang, N. Gu, T. Wang, *Nat. Nanotechnol.* **2007**, *2*, 577; g) F. Natalio, R. André, A. F. Hartog, B. Stoll, K. P. Jochum, R. Wever, W. Tremel, *Nat. Nanotechnol.* **2012**, *7*, 530; h) G. Y. Tonga, Y. Jeong, B. Duncan, T. Mizuhara, R. Mout, R. Das, S. T. Kim, Y.-C. Yeh, B. Yan, S. Hou, V. M. Rotello, *Nat. Chem.* **2015**, *7*, 597; i) C. N. Loynachan, A. P. Soleimany, J. S. Dudani, Y. Lin, A. Najer, A. Bekdemir, Q. Chen, S. N. Bhatia, M. M. Stevens, *Nat. Nanotechnol.* **2019**, *14*, 883.
- [31] N. K. Lee, Y. G. Choi, J. Y. Baik, S. Y. Han, *Blood* **2005**, *106*, 852.
- [32] V. Selvaraj, N. Nepal, S. Rogers, N. D. P. K. Manne, R. Arvapalli, K. M. Rice, S. Asano, E. Fankhanel, J. J. Ma, T. Shokuhfar, M. Maheshwari, E. R. Blough, *Biomaterials* **2015**, *59*, 160.